

Markovianity and non-Markovianity of Particle Bath with Dirac Dispersion Relation

Takano Taira, Naomichi Hatano, Akinori Nishino

Abstract

The decay rate of quantum particles in open quantum systems has traditionally been known as exponential, based on empirical predictions from experiments and theoretical predictions from the Markovian dynamics of the corresponding quantum states. However, both theoretical predictions and experimental observations suggest deviations from this exponential decay, particularly in the short and long time regimes. In this study, we explore the spontaneous emission of a single Dirac particle within an environment characterized by an energy spectrum with a gap m and an energy cutoff L . Our results reveal that high-energy structures, such as the spectral cutoff L , play a critical role in driving the short-time non-exponential decay. In contrast, the long-time decay is predominantly influenced by low-energy structures, such as the Dirac gap m . Surprisingly, we find that in the limits where the energy cutoff L is infinite and the energy gap m is zero, the decay dynamics of massless Dirac particles exhibit Markovian behavior without the need for conventional approximations like the Born-Markov approximation. This work underscores the complex interplay between particle energy properties and decay dynamics, providing new insights into quantum decay processes.

1 Introduction

The history of research on non-exponential decay in quantum systems dates back to the work in 1958 by Khalfin [9] in the context of nuclear decay, which predates the development of quantum master equations for open quantum systems, such as the Nakajima-Zwanzig [15, 22] and Gorini–Kossakowski–Sudarshan–Lindblad (GKSL) [6, 11] equations, which were developed in the 1960s and 1970s, respectively. Khalfin demonstrated a power-law decay in the long-time regime, which was experimentally confirmed as late as 2006 [20]. In 1977, Chiu, Sudarshan, and Misra [2] demonstrated a non-exponential decay in the short-time regime, which led to the prediction of the quantum Zeno effect [14], in which continuous observation of an excited state prevents the state from decaying. This was experimentally observed in 1990 [8]. In these findings, Khalfin [9], Chiu, Misra, and Sudarshan [2] utilized a theorem based on the Fourier analysis called the Paley-Wiener theorem [17], which implies that if the spectrum of the Hamiltonian occupies the entire real axis, the decay is purely exponential, and vice versa. This implies that when the spectrum of the Hamiltonian is bounded from below, the decay profile is non-exponential.

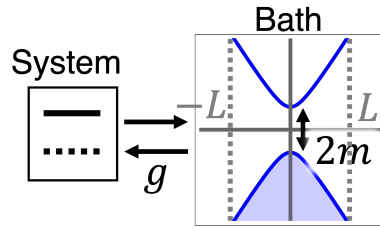
In a physical setup, it is natural to assume that the spectrum of the Hamiltonian is bounded from below; hence, according to the prediction by Khalfin, Chiu, Sudarshan, and Misra, the decay should be non-exponential in general. However, the exponential

decay is widely accepted as a standard decay profile of quantum systems, as early as in the first empirical confirmation of an exponential decay by Rutherford and Soddy in 1902 [21].

The exponential decay also follows from the GKSL equation. To see this, consider the dynamical map of the system density $\rho_S(t) = \exp(\mathcal{L}t)\rho_S(0)$, where $\rho_S(t)$ is the system density matrix at time t and \mathcal{L} is the Liouvillian superoperator of the GKSL form. The decaying profile, or the survival probability of an excited state $|1\rangle$ is given by $\langle 1|\rho_S(t)|1\rangle$. If \mathcal{L} is diagonalizable, the survival probability decays exponentially with a possible periodic oscillation. When \mathcal{L} is non-diagonalizable due to an exceptional point [13], the survival probability initially shows a power-law increase but is later suppressed by an exponential decay. In short, the GKSL equation shows an exponential decay. Since GKSL (or GKSL-type) equation follows from the assumption of semi-group property of the dynamical map, often taken as the definition of the quantum Markovianity [19], one can deduce that the *Markovian dynamics of the system implies an exponential decay*. The negation of such a statement is that the *non-exponential decay implies non-Markovian dynamics of the system*. Therefore, in a physical setup, in which the spectrum of the full Hamiltonian is bounded from below, the system's dynamics must be non-Markovian, and only with Markov and Born approximations can the Markovian dynamics be achieved.

Short-time decay profile of survival prob.

	$m = 0$	$m \neq 0$
$L < \infty$	Quadratic	Quadratic
$L \rightarrow \infty$	Exp.	Exp.



Long-time decay profile of survival prob.

	$m = 0$	$m \neq 0$
$L < \infty$	Power law decay to bound state	Power law decay to bound state
$L \rightarrow \infty$	Exp. decay to zero	Power law decay to bound state

Table 1: Two tables showing the decay profiles of the survival probability $P(t)$ for short and long time regimes. The picture shows a schematic of our model (1) with coupling g , gap m , and momentum cut off L shown.

On the other hand, it has been demonstrated analytically in electron transport in a single-electron case [7] and an interacting case [16] that the excited state decays exponentially without any approximation. This phenomenon can be attributed to the model being understood as a massless Dirac particle, whose spectrum features a Dirac cone and is unbounded. Thus, the question arises: *What happens to the decay profile when a Dirac gap opens?* This is the central question of this paper.

We will consider a simple two-level system attached to a Dirac-particle bath, schematically represented in Table 1. Our result is also summarised in Table 1, where high-energy structures, such as the cutoff L , primarily contribute to the short-time regime producing a quadratic decay, whereas low-energy structures, such as the Dirac gap m , mainly contribute to the long-time regime producing a power-law decay and localized bound states, as seen in Ref. [10, 3]. Surprisingly, the opening of the Dirac gap, which has no lower or upper bound, still induces deviations from pure exponential decay. We note that the correspondence between the gap structure of the spectrum and the survival probability was also studied in the context of quantum optics [10]

and with the tight-binding model [3] in long-time regimes. In the present work, we have extended their work to the Dirac gap m , and further analyzed the interplay with the cutoff L in both short- and long-time regimes.

Our model is mathematically similar to quantum optical models. Two key differences are that we consider a Dirac particle instead of photons and that we focus on controlling the Dirac gap to observe various non-Markovian dynamics; in quantum optics, on the other hand, the Dirac cone is typically fixed [18, 5].

Our model has a possibility for applications in photonic crystals, which can be engineered to exhibit a linear frequency dispersion [18, 5]. In this case, the spectrum of the Hamiltonian is unbounded, with negative energy states occupied by antiparticles, or holes. Therefore, our results in Table 1 suggest that such systems might exhibit Markovian dynamics without any approximations. Moreover, when the mass of the Dirac particle is finite, a gap opens in the Hamiltonian's spectrum, potentially exhibiting non-Markovian dynamics in the long-time regime. These insights suggest that controlling the spectrum's gap to regulate the Markovianity of system dynamics could benefit both quantum optics and electron systems.

In Section 2, we introduce our toy model and derive the master equation. In Section 3 we analytically investigate the master equation in the cases of $m > 0, L \rightarrow \infty$ and $m = 0, L < \infty$. In Section 4, we numerically investigate the most general case $m > 0, L < \infty$.

2 Survival probability of two-level system with half-filled Dirac environment

In this section, we will introduce the model and obtain a non-Markovian master equation of the system, starting from the Schrödinger equation of the full system.

2.1 Model

We introduce a simple toy model, designed to capture the essence of the interplay between the Dirac particle's mass and the resulting dynamical behavior:

$$H_{\text{full}} = \omega_0 \sigma_+ \sigma_- + H_D + (\sigma_+ \otimes B + \sigma_- \otimes B^\dagger). \quad (1)$$

The first term of the full Hamiltonian (1) is the two-level Hamiltonian, which we refer to as the *two-level system* with the states $\{|0\rangle_S, |1\rangle_S\}$. We take the level difference ω_0 to be real and constant. The operators $\sigma_+ := (\sigma_x - i\sigma_y)/2$ and $\sigma_- := (\sigma_x + i\sigma_y)/2$ are the creation and annihilation operators of the two-level system, which satisfies the fermionic anti-commutation relations:

$$\{\sigma_-, \sigma_+\} = \{\sigma_-, \sigma_+\} = 1, \quad \{\sigma_-, \sigma_-\} = \{\sigma_+, \sigma_+\} = 0. \quad (2)$$

The second term of Eq. (1) is the half-filled Dirac Hamiltonian, which we refer to as the *environment*:

$$: H_D := \int_{-L}^L dp \omega_p (b_p^\dagger b_p - c_p c_p^\dagger) \quad \text{with} \quad |\text{vac}\rangle_B := \prod_p c_p^\dagger |0\rangle, \quad (3)$$

where $L > 0$ is the cutoff on the momentum space. We note that the normal ordering is taken with respect to the vacuum state $|\text{vac}\rangle_B$. The operators b_p^\dagger and c_p^\dagger are

creation operators of electrons with the same dispersion relation ω_p , satisfying the commutation relations:

$$\{b_p, b_k^\dagger\} = \{c_p, c_k^\dagger\} = \delta(p - k), \quad (4)$$

$$\{b_p, b_k\} = \{c_p, c_k\} = \{b_p, c_k\} = \{b_p, c_k^\dagger\} = 0, \quad (5)$$

where curly brackets indicate the anti-commutator. The dispersion relation for massive and massless particles is given by

$$\text{massive} : \omega_p = \sqrt{p^2 + m^2}, \quad (6)$$

$$\text{massless} : \omega_p = |p|. \quad (7)$$

Finally, the last two terms of Eq. (1) represent the interaction between the two-level system and the environment. The third term $\sigma_+ \otimes B$, where $B := \int_{-L}^L dp g_p B_p$, $B_p := b_p + c_p^\dagger$, creates the particle in the two-level system and at the same time either destroys a particle by b_p or creates a particle by c_p^\dagger in the environment, preserving the overall particle number. The coupling parameter g_p captures the details of the interaction. Throughout this paper, we consider the case of a simple uniform coupling $g_p = g$.

2.2 Master equation

Next, let us find the master equation associated with our model. For brevity, let us consider the following abbreviation of the composite states:

$$|0\text{vac}\rangle := |0\rangle_S \otimes |\text{vac}\rangle_B, \quad (8)$$

$$|1\text{vac}\rangle := |1\rangle_S \otimes |\text{vac}\rangle_B. \quad (9)$$

Note that $|1\text{vac}\rangle = \sigma^+ |0\text{vac}\rangle$. Following the same procedure as in Refs. [4, 1], we let the initial state have a single particle in the excited state of the two-level system:

$$|\phi(0)\rangle := \phi(0) |1\text{vac}\rangle. \quad (10)$$

Given that the full system (1) is assumed to be closed, the particle number is conserved. This can be checked by calculating the commutation relation between the Hamiltonian (1) and the number operator. Therefore, the state at an arbitrary time t must be given by

$$|\phi(t)\rangle := \phi(t) |1\text{vac}\rangle + \int_{-L}^L dp \phi_p(t) b_p^\dagger |0\text{vac}\rangle + \int_{-L}^L dp \psi_p(t) c_p |0\text{vac}\rangle. \quad (11)$$

We require the coefficients to satisfy the normalization condition:

$$|\phi(t)|^2 + \int_{-L}^L dp |\phi_p(t)|^2 + \int_{-L}^L dp |\psi_p(t)|^2 = 1. \quad (12)$$

Inserting the Ansatz (11) to the Schrödinger equation of the full system $i\hbar\partial_t |\psi\rangle = H_{\text{full}} |\psi\rangle$, we find the following coupled first-order equations of the coefficients ϕ , ϕ_p and ψ_p :

$$i\hbar \frac{d\phi(t)}{dt} = \omega_0 \phi(t) + g \int_{-L}^L dp (\phi_p(t) + \psi_p(t)), \quad (13)$$

$$i\hbar \frac{d\phi_p(t)}{dt} = \omega_p \phi_p(t) + g\phi(t), \quad (14)$$

$$i\hbar \frac{d\psi_p(t)}{dt} = -\omega_p \psi_p(t) + g\phi(t). \quad (15)$$

In order to eliminate the first term on the right-hand side of each equation, we introduce the new functions $\Phi(t) := e^{i\omega_0 t/\hbar} \phi(t)$, $\Phi_p(t) := e^{i\omega_p t/\hbar} \phi_p(t)$ and $\Psi_p(t) := e^{-i\omega_p t/\hbar} \psi_p(t)$. The coupled first-order equations now take the following form:

$$i\hbar \frac{d\Phi(t)}{dt} = g \int_{-L}^L dp e^{i\hbar\omega_0 t} \left(\Phi_p(t) e^{-\frac{i}{\hbar}\omega_p t} + \Psi_p(t) e^{\frac{i}{\hbar}\omega_p t} \right), \quad (16)$$

$$i\hbar \frac{d\Phi_p(t)}{dt} = g e^{-\frac{i}{\hbar}(\omega_0 - \omega_p)t} \Phi(t), \quad (17)$$

$$i\hbar \frac{d\Psi_p(t)}{dt} = g e^{-\frac{i}{\hbar}(\omega_0 + \omega_p)t} \Phi(t). \quad (18)$$

The last two equations can be solved, yielding the following equations:

$$\Phi_p(t) = \frac{1}{i\hbar} g \int_0^t ds e^{-\frac{i}{\hbar}(\omega_0 - \omega_p)s} \Phi(s) + \Phi_p(0), \quad (19)$$

$$\Psi_p(t) = \frac{1}{i\hbar} g \int_0^t ds e^{-\frac{i}{\hbar}(\omega_0 + \omega_p)s} \Phi(s) + \Psi_p(0). \quad (20)$$

Inserting these to Eq. (16), the explicit form of the coefficient $\Phi(t)$ is found by solving the following non-Markovian master equation:

$$\begin{aligned} \frac{d\Phi(t)}{dt} = & -\frac{1}{\hbar^2} \int_0^t ds e^{\frac{i}{\hbar}\omega_0(t-s)} \Phi(s) g^2 \int_{-L}^L dp \cos \left[\omega_p \frac{t-s}{\hbar} \right] \\ & - \frac{i}{\hbar} g^2 \int_{-L}^L dp e^{\frac{i}{\hbar}\omega_0 t} \left(e^{-\frac{i}{\hbar}\omega_p t} \Phi_p(0) + e^{\frac{i}{\hbar}\omega_p t} \Psi_p(0) \right). \end{aligned} \quad (21)$$

Notice that with our initial condition (10), the second term of the above equation vanishes. We will refer to the p integral part of the first term as the *memory kernel*.

The norm squared of the solution to the above master equation is the survival probability of the particle at the state $|1_{\text{vac}}\rangle$. To see this, we will follow the procedure in Sections 10.1.1 and 10.1.2 of Ref. [1]. We first define the system density matrix as

$$\rho_S(t) := \text{Tr}_B (|\phi(t)\rangle \langle \phi(t)|), \quad (22)$$

where the trace over B is defined as

$$\text{Tr}_B (\rho) := {}_B \langle \text{vac} | \rho | \text{vac} \rangle_B + \sum_p {}_B \langle \text{vac} | b_p \rho b_p^\dagger | \text{vac} \rangle_B + \sum_p {}_B \langle \text{vac} | c_p^\dagger \rho c_p | \text{vac} \rangle_B. \quad (23)$$

Using the normalization condition (12), we arrive at the system density matrix of the form

$$\begin{aligned} \rho_S(t) &= (1 - |\phi(t)|^2) |0\rangle_{SS} \langle 0| + |\phi(t)|^2 |1\rangle_{SS} \langle 1| \\ &= \begin{pmatrix} |0\rangle_S & |1\rangle_S \end{pmatrix} \begin{pmatrix} 1 - |\phi(t)|^2 & 0 \\ 0 & |\phi(t)|^2 \end{pmatrix} \begin{pmatrix} \langle 0|_S \\ \langle 1|_S \end{pmatrix}. \end{aligned} \quad (24)$$

The survival probability of the qubit state $|1\rangle_S$ is therefore given by

$$P(t) := |\langle 1 | \rho_S(t) | 1 \rangle| = |\phi(t)|^2 = |\Phi(t)|^2. \quad (25)$$

The last equality follows from the definition that ϕ and Φ are different only up to the phase. This quantity's physical meaning is the particle's probability at the state $|1\rangle_S$ to remain or return to the original state $|1\rangle_S$ after time t .

To solve the master equation (21), we will utilize the Laplace transform. First, for brevity, let us introduce the memory kernel $\mathcal{K}(t)$ to rewrite the master equation (21):

$$\frac{d\Phi(t)}{dt} = -\frac{g^2}{\hbar^2} \int_0^t ds \Phi(s) \mathcal{K}(t-s), \quad \mathcal{K}(\tau) := e^{\frac{i}{\hbar}\omega_0\tau} \int_{-L}^L dp \cos\left(\omega_p \frac{\tau}{\hbar}\right). \quad (26)$$

After applying the Laplace transform detailed in Appendix C, we find the formal solution to the master equation (21):

$$\Phi(t) = e^{\frac{i}{\hbar}\omega_0 t} \lim_{R \rightarrow \infty} \int_{-iR+\sigma}^{iR+\sigma} \frac{dz}{2\pi i} e^{z\frac{t}{\hbar}} \left(z + i\omega_0 + 2g^2 \frac{z \operatorname{Arctan}\left(\frac{L}{\sqrt{m^2+z^2}}\right)}{\sqrt{m^2+z^2}} \right)^{-1} \Phi(0). \quad (27)$$

3 Spectral structure and Markovianity

The integral in the solution (27) can be evaluated numerically. It shows a t^{-2} decay in a short time, an exponential decay in mid-time, and a power law decay with oscillation in a long time. In this section, we investigate the relation between these non-exponential behaviors and the spectrum structure. We will find that the low-energy structure, such as the energy gap, corresponds to the long-time behavior, whereas the high-energy structure, such as the cutoff, corresponds to the short-time behavior; see Table 1 and for the long-time behavior in Table 1, where, lightly shaded regions indicate an exponential decay, while darkly shaded regions indicate a non-exponential decay.

3.1 Low energy structure and Markovianity: $m > 0, L \rightarrow \infty$ limit

First, consider the limit $L \rightarrow \infty$, which removes the high-energy cutoff and leaves the low-energy energy gap $2m$. In this case, the Arctan function in the integrand of Eq. (27) becomes $\pi/2$, and hence the solution (27) is reduced to the following relatively simple form:

$$\Phi(t) = e^{\frac{i}{\hbar}\omega_0 t} \lim_{R \rightarrow \infty} \int_{-iR+\sigma}^{iR+\sigma} \frac{dz}{2\pi i} e^{z\frac{t}{\hbar}} F(z) \Phi(0), \quad (28)$$

where we have defined the complex function $F(z)$ as

$$F(z) := \left(z + i\omega_0 + g^2 \frac{\pi z}{\sqrt{m^2+z^2}} \right)^{-1}. \quad (29)$$

Notice that the function $F(z)$ depends on the square root of the complex variable z , which can only be smoothly defined on the Riemann surface. Let us denote the two Riemann sheets as \mathcal{R}_\pm , where labeling indicates the sign $\sqrt{-1} = \pm i$. We draw a branch cut from the point $z = \pm im$ going off to negative infinity as shown in Fig. 1(a). Note that the infinity is not the branch points of $\sqrt{m^2+z^2}$.

Typically, the above integral is computed using the Cauchy residue theorem, simplifying the integral to the sum of the residues of the integrand. However, due to the branch cut in the function $F(z)$, not all poles are located on the first Riemann sheet, preventing a straightforward summation of all pole contributions.

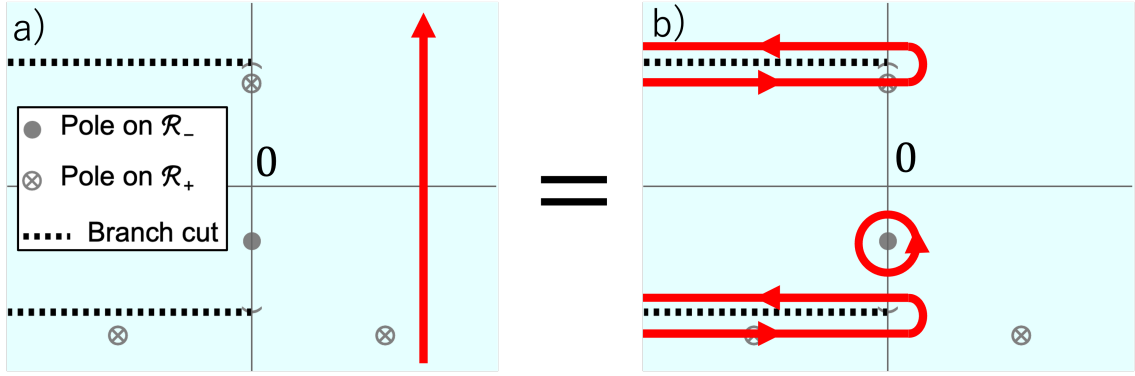


Figure 1: Panel (a) shows the contour, branch cuts, and poles of the Bromwich integral (28), which is equivalent to the contour shown in panel (b).

In order to find the correct locations of the poles, we reexpress the function as follows:

$$\begin{aligned}
 F(z) &= \frac{\sqrt{m^2 + z^2}}{(z + i\omega_0)\sqrt{m^2 + z^2} + g^2\pi z} & (30) \\
 &= \frac{\sqrt{m^2 + z^2}}{(z + i\omega_0)\sqrt{m^2 + z^2} + g^2\pi z} \frac{(z + i\omega_0)\sqrt{m^2 + z^2} - g^2\pi z}{(z + i\omega_0)\sqrt{m^2 + z^2} - g^2\pi z} \\
 &= \frac{(z + i\omega_0)(m^2 + z^2) - g^2\pi z\sqrt{m^2 + z^2}}{\mathcal{P}(z)}, & (31)
 \end{aligned}$$

where $\mathcal{P}(z) = (z + i\omega_0)^2(m^2 + z^2) - g^4\pi^2 z^2$ represents the fourth-order polynomial in the denominator of the final expression. The zeros of $\mathcal{P}(z)$ determine the four poles of the integrand. Analyzing the discriminant of the polynomial, which can be evaluated explicitly, reveals the presence of two purely imaginary solutions, denoted by $z_0, z_1 \in i\mathbb{R}$, and a pair of complex solutions, z_{\pm} , where $z_+ = -(z_-)^*$. Imposing the constraint that parameters ω_0, m, g are all positive, one can show explicitly that the imaginary parts of z_0, z_1 are negative and positive, respectively. Notice that z_{\pm} may also be purely imaginary under certain conditions. The regime allowing for purely imaginary poles z_{\pm} can be deduced by examining the discriminant of $\mathcal{P} = 0$, where the phase diagram, illustrated in Fig. 2, depicts a transition from four imaginary poles to two imaginary and two complex poles. This transition point is known as the exceptional point.

Going back to the expression of the integrand (30), one can show by using the fact that on the principle Riemann sheet \mathcal{R}_+ , the square root is defined as $\sqrt{-1} = i$, only z_0 is the pole of the function $F(z)$. Other zeros of $\mathcal{P}(z)$ are poles of $F(z)$ only on the second Riemann sheet \mathcal{R}_- , where $\sqrt{-1} = -i$:

$$\begin{aligned}
 z_0 &\in -i\mathbb{R}_{\geq 0} && \text{on } \mathcal{R}_+, \\
 z_1 &\in i\mathbb{R}_{\geq 0}, \quad z_+ = -(z_-)^* && \text{on } \mathcal{R}_-.
 \end{aligned} \tag{32}$$

This would lead to the numerator of Eq. (31) vanishing for zeros z_1, z_{\pm} . Note that contrary to the conventional Markovian dynamics, where the exceptional point of the Lindbladian operator shows a sudden change in the dynamical behavior of the state, in our case, the exceptional point in the parameter space shown in Fig. 2 does not affect to the system's dynamics.

We are now in a position to evaluate the Bromwich integral in Eq. (28), where its contour and locations of the poles and branch cuts are shown in Fig. 1(a). The

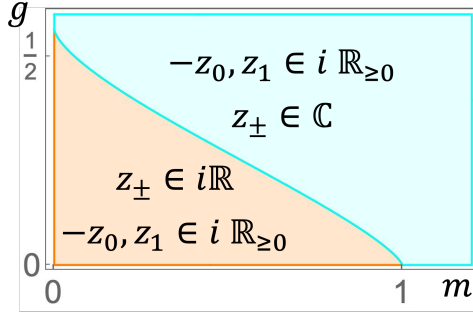


Figure 2: Phase diagram of solutions to the fourth-order polynomial $\mathcal{P}(z) = (z + i\omega_0)^2(m^2 + z^2) - g^4\pi^2 z^2$, where we put $\hbar = \omega_0 = 1$.

Bromwich contour in Eq. (28), shown in Fig. 1(a) is equivalent to the contour in Fig. 1(b). This can be shown by using the Cauchy theorem; see details in Appendix B. Therefore the Bromwich integral in Eq. (28) is decomposed to the contributions from the pole z_0 on the first Riemann sheet and the contour around the branch cut:

$$\Phi(t) = e^{\frac{i}{\hbar}\omega_0 t} \left[\oint_{z_0} \dots + \int_{\text{BC}} \dots \right] \Phi(0). \quad (33)$$

Applying the Cauchy residue theorem at the pole z_0 , we obtain

$$\oint_{z_0} \dots = \text{Res}(F(z)e^{zt}, z_0) = \frac{(z_0 + i\omega_0)(m^2 + z_0^2) - g^2\pi z_0 \sqrt{m^2 + z_0^2}}{(z_0 - z_1)(z_0 - z_+)(z_0 - z_-)} e^{z_0 t} \quad (34)$$

Given that z_0 is purely imaginary, this value does not contribute to the system's decay but to a bound state.

Note that if we set $\omega_0 = 0$ and evaluate the residue, we find the following simple expression:

$$\oint_{z_0} \dots = \text{Res}(F(z)e^{zt}, z_0) = \frac{m}{m + \pi g^2}. \quad (35)$$

Note that this expression cannot be obtained by simply taking the limit $\omega_0 \rightarrow 0$ in Eq. (34), as one must take the limit there is a limit $\omega_0 \rightarrow 0$, before calculating the residue.

Next, let us consider the branch cut contribution. Let $F_{\pm}(z)$ denote the integrand of Eq. (28) on the Riemann sheets \mathcal{R}_{\pm} , respectively. We explicitly have

$$F_{\pm}(z) = \frac{(z + i\omega_0)(m^2 + z^2)}{\mathcal{P}(z)} \pm \frac{-g^2\pi z \sqrt{m^2 + z^2}}{\mathcal{P}(z)}, \quad (36)$$

where the square-root function in the above expression is assumed to be the principal branch with $\sqrt{-1} = i$.

The upper part of the branch-cut contribution in Fig. 1(b) is given by

$$\int_{-R+im}^{im} \frac{dz}{2\pi i} F_+(z) e^{z\frac{t}{\hbar}} + \int_{im}^{-R+im} \frac{dz}{2\pi i} F_-(z) e^{z\frac{t}{\hbar}} \quad (37)$$

$$\begin{aligned} &= \int_{-R+im}^{im} \frac{dz}{2\pi i} (F_+(z) - F_-(z)) e^{z\frac{t}{\hbar}} \\ &= \int_{-R+im}^{im} \frac{dz}{2\pi i} A(z) e^{z\frac{t}{\hbar}} \\ &= \int_{-R}^0 \frac{dw}{2\pi i} A(w+im) e^{w\frac{t}{\hbar}} e^{im\frac{t}{\hbar}}, \end{aligned} \quad (38)$$

and $A(z) := (-2g^2\pi z\sqrt{m^2+z^2})/\mathcal{P}(z)$, where we have performed a coordinate transformation $z = w+im$. The lower part of the branch cut contribution can be calculated in a similar way, and thus we find the full branch-cut contribution in the form

$$\int_{\text{BC}} \dots = \lim_{R \rightarrow \infty} \int_{-R}^0 \frac{dw}{2\pi i} \left(A(w+im) e^{im\frac{t}{\hbar}} - A(w-im) e^{-im\frac{t}{\hbar}} \right) e^{w\frac{t}{\hbar}}. \quad (39)$$

For the rest of this paper, we will refer to Eq. (34) and the integral form of Eq. (39) inserted into Eq. (33) as the "exact solution."

Given explicit expression of the integral, we turn to the large-time asymptotic analysis outlined in Ref. [3]. First, we change the complex variable from ω to τ , related via $wt \equiv \tau$. The integrand can be expanded as a series of $1/t$. The lowest-order term is $1/\sqrt{t}$, which after evaluation gives

$$\int_{\text{BC}} \dots = \frac{1}{g^2\sqrt{m}} \left(\cos\left(\frac{mt}{\hbar}\right) + \sin\left(\frac{mt}{\hbar}\right) \right) \left(\frac{\hbar}{\pi t}\right)^{3/2} + \mathcal{O}\left(\frac{1}{t^{5/2}}\right). \quad (40)$$

Therefore, we find the asymptotic contribution of a branch cut to be the power-law decay.

In Fig. 3, we present our findings. Figure 3 illustrates the survival probability $P(t) = |\Phi(t)|^2$ over the entire time range. We note that $P(t)$ decays to a constant value over time, which is the residue of the pole z_0 :

$$|\text{Res}(F(z)e^{zt}, z_0)\Phi(0)|^2. \quad (41)$$

Given that the pole z_0 is always pure imaginary, the magnitude of this residue is independent of time, allowing the survival probability to maintain a finite value indefinitely. The constant value predicted by the residue is depicted as a horizontal red dashed line in Fig. 3(a).

The short-time dynamics are depicted in Fig. 3(b), where we used a log-log plot to display $1 - P(t)$ for the exact solution (33). The slope of the straight line on this plot represents the power governing the decay. From Fig. 3(b), it is evident that the exact solution exhibits a linear decay at short times. This observation suggests that the quantum Zeno effect (see Appendix A), which requires a quartic short-time decay, is absent when $L \rightarrow \infty$. Consequently, we infer that the quantum Zeno effect arises from the spectral bounds of the system rather than the gap structure. We will see in the next sub section 3.2 that a finite value of L introduces a new pair of poles, which gives rise to the quartic decay.

Finally, to see the decay in the long-time regime, we subtract the bound-state contribution from the exact solution (33) and plot only the branch cut contribution

in Fig. 3(c). The dashed lines in Fig. 3(c) indicate the approximations up to order $t^{-3/2}$ and up to $t^{-5/2}$ given by Eq. (40). We observe a good agreement with the exact solution beyond $t = 10$, and from Fig. 3(c), we observe that the approximation gives a good prediction beyond $t = 10$.

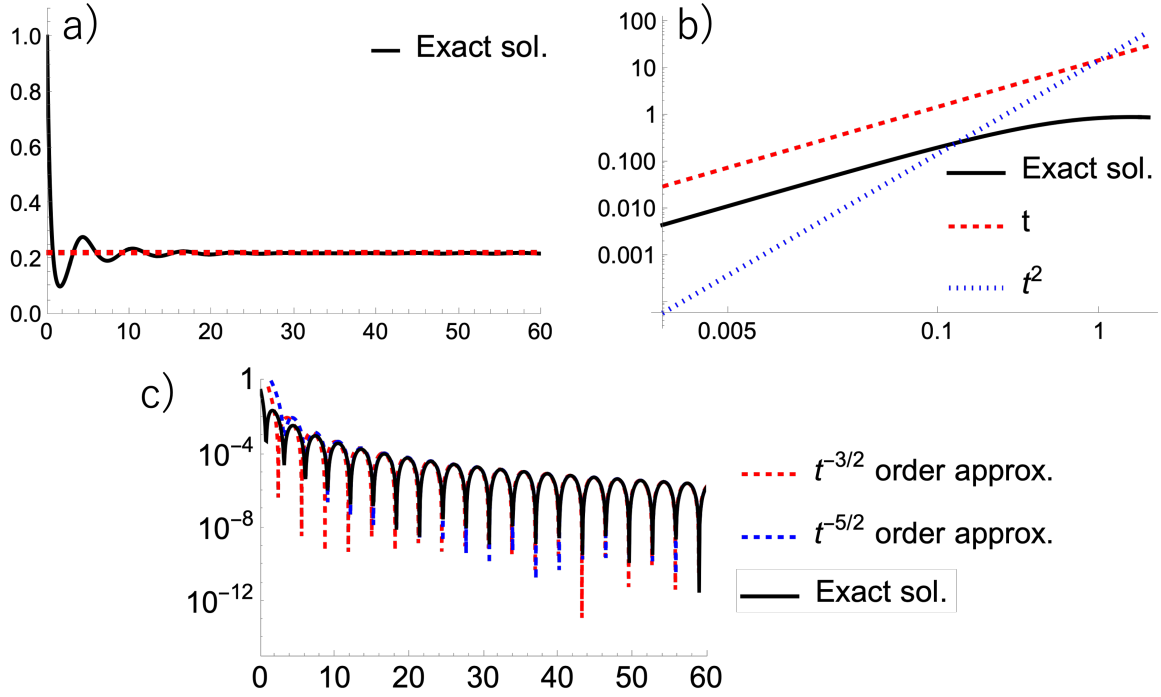


Figure 3: All three panels are showing the plot for $\hbar = 1, \omega_0 = 0.1, m = 1, g = 0.6$ in different time regimes. (a) the plot of the survival probability $P(t)$ given by Eq. (33). The horizontal red dashed line indicates the absolute value squared of the pole contribution (34) (b) the log-log plot of $1 - P(t)$ for the exact solution (33), plotted along t and t^2 . (c) the log plot of the numerical solution and approximations up to $t^{-3/2}$ and up to $t^{-5/2}$ in Eq. (40).

3.2 High energy structure and Markovianity: $m = 0, L < \infty$ case

To investigate the high-energy contribution for $L < \infty$, let us remove the low-energy contribution by taking $m = 0$. The formal solution is simplified to

$$\begin{aligned} \Phi(t) &= e^{\frac{i}{\hbar}\omega_0 t} \lim_{R \rightarrow \infty} \int_{-iR+\sigma}^{iR+\sigma} \frac{dz}{2\pi i} e^{z\frac{t}{\hbar}} \left(z + i\omega_0 + 2g^2 \text{Arctan} \left(\frac{L}{z} \right) \right)^{-1} \Phi(0) \\ &= e^{\frac{i}{\hbar}\omega_0 t} \lim_{R \rightarrow \infty} \int_{-iR+\sigma}^{iR+\sigma} \frac{dz}{2\pi i} e^{\frac{1}{\hbar}g^2 z t} \left(z + ia + 2\text{Arctan} \left(\frac{b}{z} \right) \right)^{-1} \Phi(0), \end{aligned} \quad (42)$$

where in the last line, we have rescaled the integration variable from z to z/g^2 and introduced new parameters $a \equiv \omega_0/g^2$ and $b \equiv L/g^2$.

The integrand now has a different type of Riemann surface, where branch points are located at $z = \pm ib = \pm iL/g^2$ and ∞ . To find the poles, we must find the solutions to the following equation:

$$z + ia + 2\text{Arctan} \left(\frac{b}{z} \right) = z + ia - i\text{Log} \left(\frac{z + ib}{z - ib} \right) = 0. \quad (43)$$

This transcendental equation cannot be solved directly. However, by defining $w = -iz - b$, $r = -\exp(-a - b)$, and $\alpha = -2br$, we can rewrite it as

$$we^w + rw = \alpha, \quad r \in [-1, 0), \quad \alpha \in (0, 2b]. \quad (44)$$

This is a rewritten form of the generalized Euler-Lambert or r -Lambert equation [12]. The solution to the above equation is denoted by the r -Lambert function of the parameter α : $W_r(\alpha)$. The branch structure of this function has been rigorously analyzed in Ref.[12], revealing that there are only two real solutions on the principal Riemann sheet, which translate to purely imaginary solutions in the z plane. While infinitely many solutions exist for the above equation, only two real solutions can be found on the principle Riemann sheet for $\alpha \in (0, 2b)$.

From the above analysis, we find two pure imaginary poles ix_1 and $-ix_2$, where $x_1, x_2 > b$, and branch cut of the integrand of Eq. (42). Two examples of poles and branch points locations are shown in Fig.4(a) for parameters $L = 2, g = 1, \omega_0 = 0$, and in Fig.4(b) for $L = 2, g = 1, \omega_0 = 8$. Notice that locations of poles are almost in complex conjugate pairs in Fig.4(a) and unbalanced in Fig.4(b).

Following the trick similar to the one in the previous section, we can rewrite the Bromwich integral into the contributions from the poles and branch cut:

$$\Phi(t) = e^{\frac{i}{\hbar}\omega_0 t} \left[\oint_{ix_1} \dots + \oint_{-ix_2} \dots + \int_{BC} \dots \right] \Phi(0), \quad (45)$$

where ix_1 and $-ix_2$ are two purely imaginary solutions to Eq. (43) with $x_1, x_2 > b$.

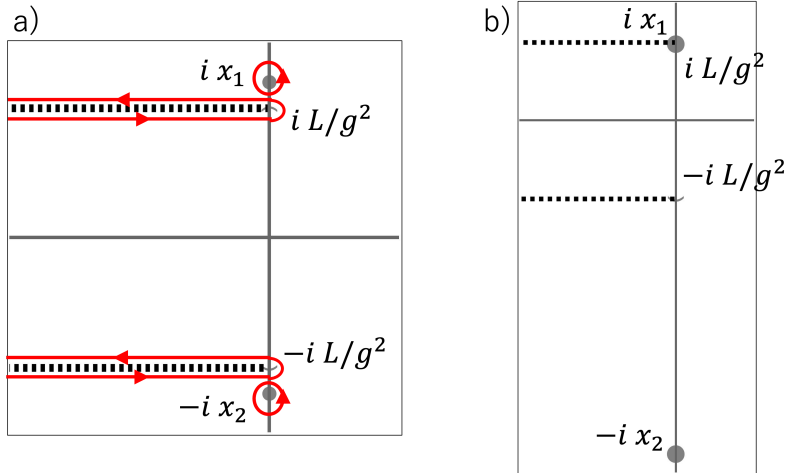


Figure 4: Panel (a) and (b) show the plot of poles on the principle Riemann surface for $L = 2, g = 1, \omega_0 = 0$ and $L = 2, g = 1, \omega_0 = 8$ respectively.

3.2.1 Pole contributions

Let us look into the contribution from the poles, starting with the upper pole:

$$\oint_{ix_1} \dots = \text{Res} [F(z)e^{zt}, ix_1] = \lim_{z \rightarrow ix_1} \frac{(z - ix_1) e^{zt}}{z + i\frac{\omega_0}{\hbar} + \frac{2g^2}{\hbar} \text{Arctan} \left(\frac{L}{zh} \right)}. \quad (46)$$

This limit is challenging to evaluate, as the denominator cannot be expressed in polynomial form. To overcome this, we apply the l'Hôpital's rule, which equates the

limit of a fraction to the limit of the fraction of derivatives, thereby simplifying the calculation of the residue:

$$\oint_{ix_1} \dots = \lim_{z \rightarrow ix_1} \frac{(z - ix_1) e^{zt}}{z + i\frac{\omega_0}{h} + \frac{2g^2}{h} \text{Arctan}\left(\frac{L}{zh}\right)} = \frac{(x_1 - b)(b + x_1) e^{\frac{ig^2 tx_1}{h}}}{x_1^2 - (b - 2)b}, \quad (47)$$

where $b = L/g^2$.

Similarly, the contribution from the lower pole is determined by the l'Hôpital's rule again. We derive the combined contribution of both poles, $\text{Pole}(t) := \oint_{ix_1} + \oint_{-ix_2}$ as

$$\text{Pole}(t) = \frac{(x_1 - b)(b + x_1) e^{i\frac{g^2 x_1 t}{h}}}{x_1^2 - (b - 2)b} + \frac{(x_2 - b)(b + x_2) e^{-i\frac{g^2 x_2 t}{h}}}{x_2^2 - (b - 2)b}. \quad (48)$$

Notice that when two poles ix_1 and $-ix_2$ are almost complex conjugate to each other as seen in Fig.4(a), which means $x_1 \sim x_2$, then the above pole contribution is reduced to the periodic contribution:

$$\text{Pole}(t) \sim \frac{2(x_1^2 - b^2) \cos\left(\frac{g^2 x_1 t}{h}\right)}{x_1^2 - (b - 2)b}. \quad (49)$$

When one of the poles is close to the branch point but one is away from the branch point as shown in the Fig.4(b), then the pole contribution gives bound-state contribution

$$\text{Pole}(t) \sim \frac{(x_2^2 - b^2) e^{-i\frac{g^2 x_2 t}{h}}}{x_2^2 - (b - 2)b}. \quad (50)$$

Therefore, the pole contribution shows no decay process and only bound-state or periodic contribution for different parameter values.

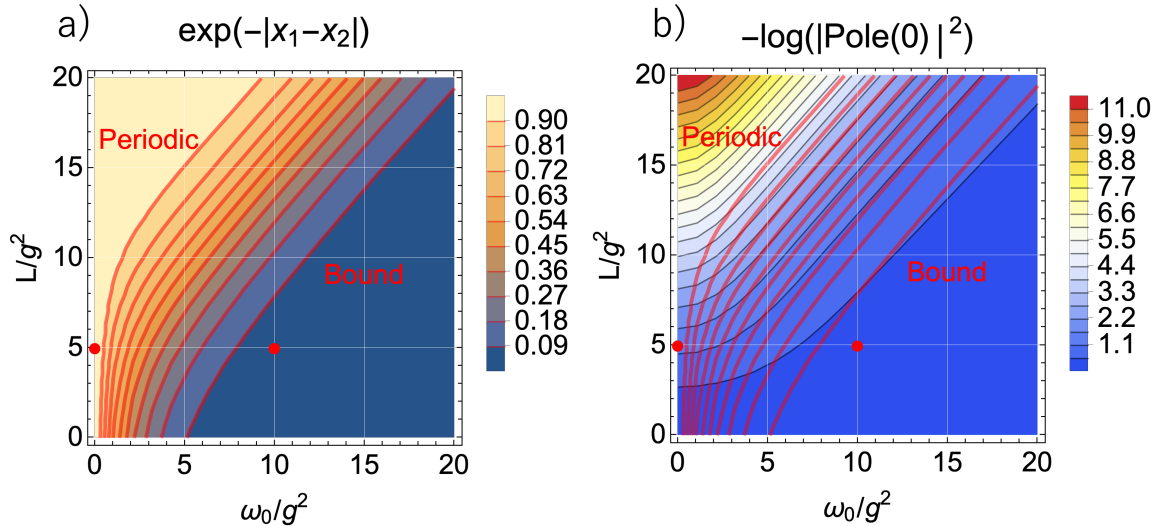


Figure 5: (a) Contour plot of $\exp(-|x_1 - x_2|)$, showing the periodic regions where $x_1 \sim x_2$ and bound region where x_1 and x_2 are different. Two points indicate the parameter choices for the plot of the survival probability in Fig.6. (b) Contour plot of $-\log(|\text{Pole}(0)|^2)$, with overlap of the contour lines of $\exp(-|x_1 - x_2|)$.

The above analysis reveals that the periodicity and bound-state behavior of the survival probability depend on the distances from each pole, ix_1 and $-ix_2$, to the branch points iL/g^2 and $-iL/g^2$. Therefore, to investigate the parameter regimes where periodic or bound-state behavior is observed, we plot the contour of the function $e^{-|x_1-x_2|}$ over the parameters $a = \omega_0/g^2$ and $b = L/g^2$ as shown in Fig.5(a). Notice the smooth transition from the periodic to the bound-state contribution for $(\omega_0/g^2, L/g^2) = (0, 5)$ to $(\omega_0/g^2, L/g^2) = (10, 5)$ with corresponding survival probabilities shown in Fig.6(a) and Fig.6(b), respectively.

Comparing two contour plots Fig.5(a) and Fig.5(b), one may notice that most of the periodic region shown in Fig.5(a) coincide with the yellow to red region of Fig.5(b). Only periodic region that is within 10^0 to 10^{-5} amplitude in Fig.5(b) is for smaller values of ω_0/g^2 . As an example, we have taken $(\omega_0/g^2, L/g^2) = (0, 5)$, which indeed shows dominating periodic contribution in Fig.6(a). By increasing ω_0/g^2 to $(\omega_0/g^2, L/g^2) = (10, 5)$, we observe the transition to the bound-state contribution in Fig.6(a). However, the bound-state contribution still shows small oscillatory behaviour shown in the small box in Fig.6(b).

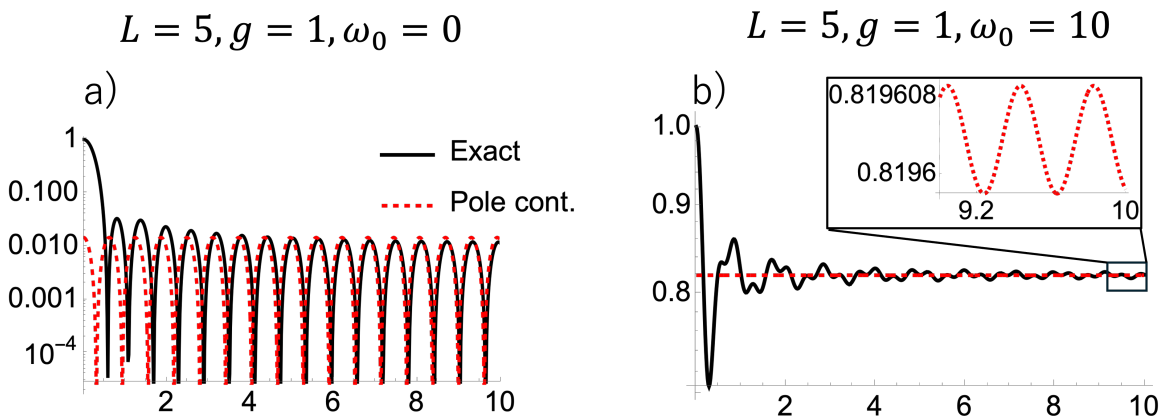


Figure 6: Log plot of the numerical evaluation of the survival probability and the pole contribution (48). Each of four plots corresponds to four points of the parameters indicated in the phase diagram 5

3.2.2 Branch cut contribution

For the branch cut contribution, we resort to numerical analysis by subtracting the analytical pole contribution shown in Eq. (48) from the full numerical evaluation of the integral (42). Two log-log plots in the Fig.7 show the branch cut contributions for two parameter values given in Fig. 5. In both cases, we observe power law decay of t^{-2} , similar to what was observed in the previous section.

Finally, we comment on the distance between the poles and branch points. We note that it was also analyzed in Ref.[3], in which the authors identify the distance with a power law decay of the survival probability. We note that this structure differs from what is seen in Section 3.1, where the distance was between the two branch points rather than the branch point and the pole. The distance can be associated with our phase diagram with the quantities $e^{-|x_1-x_2|}$. This means that the lighter the green is on the phase diagram, the wider the distance between the pole and the branch point.

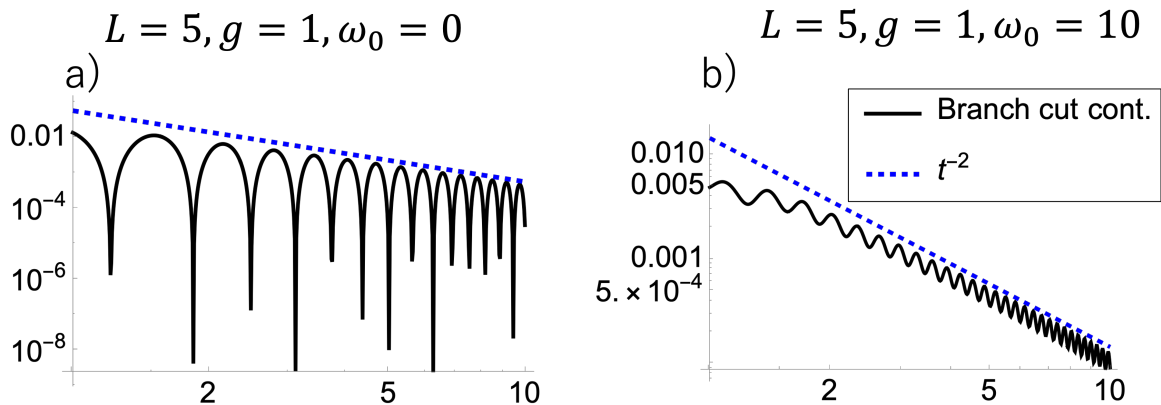


Figure 7:

4 Spectral structure and Markovianity: Numerics for $L < \infty$ and $m > 0$

In this section, we numerically consider the case $L < \infty$ and $m \neq 0$. Note that the exact analysis of this case is challenging as one is required to directly analyze the poles and branch-cut structure of the integrand in Eq. (27), which is a transcendental equation involving a square root.

We have plotted the numerical solution of the inverse Laplace transform (27) in Fig.8. We observe from Fig.8(b) that when the gap is open with $m = 1$, the long-time behavior remains almost unchanged, even when $L \rightarrow \infty$. When the gap is zero, we observed a variety of dynamical behavior in different parameter regimes shown in Fig.6. The effect of L can be seen only in the short-time regime, where in the $L \rightarrow \infty$ case, the quadratic decay becomes linear. In conclusion, we observe that the dynamical behavior observed in Section 3 manifest collectively in Fig.8.

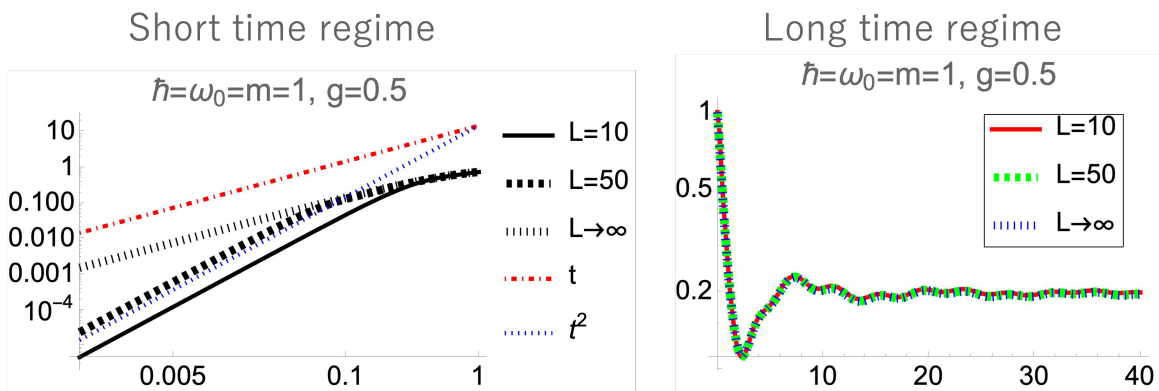


Figure 8: Numerical plot of the survival probability $P(t)$ Eq. (27) with parameters $\hbar = \omega_0 = m = 1, g = 0.5$ with different cutoff values. Panel (a) shows the log-log plot of the quantity $1 - P(t)$. Panel (b) shows the log plot of the quantity $P(t)$

5 Conclusion

We have considered the Markovianity and non-Markovianity of the Dirac particle in the context of the survival probability. For our simple toy model in Eq. (1), we have

observed that the low energy structure, such as the Dirac gap m , has no effect in the short time regime as shown in Fig.8(a). On the other hand, in the long-time regime, we observed a transition from exponential decay to power law decay as you open the Dirac gap, as shown in Table 1. We have further performed a parameter space analysis for $m \neq 0, L \rightarrow \infty$ in Fig.2 and $m = 0, L < \infty$ in Fig.5. In particular, we have identified the transition from the periodic to bound-state behavior of the survival probability in $m = 0, L < \infty$ case.

For future perspective, we aim to extend our result to the mixed state, where Schrödinger equation is replaced with the von Neumann equation. Furthermore, the control of long-time dynamics by the gap structure of the spectrum may have potential applications in quantum information and quantum optics.

A Quantum Zeno Effect

The quantum Zeno effect is a seemingly paradoxical phenomenon in quantum mechanics, theoretically proposed by Misra and Sudarshan [14]. It states that a decaying quantum state under continuous observation leads to a non-decaying probability over time. To elucidate, consider a Hamiltonian H with a bounded spectrum and an unstable state $|M\rangle$ as the initial state. Defining the survival probability $Q(t) := |\langle M | e^{-iHt/\hbar} | M \rangle|^2$. Assuming the Hamiltonian's expectation value with respect to the initial state $|M\rangle$ is finite: $\langle M | H | M \rangle < \infty$, it can be deduced that $dQ(t)/dt|_{t=0} = 0$. By segmenting the time interval into short n time slices and performing a projective measurement at each slice, the survival probability becomes $Q(t/n)^n$. In the scenario of continuous measurement, as n approaches infinity, the following is derived:

$$\lim_{n \rightarrow \infty} Q \left(\frac{t}{n} \right)^n = \lim_{n \rightarrow \infty} \left(1 + \frac{1}{2} \frac{d^2 Q(0)}{dt^2} \left(\frac{t}{n} \right)^2 \right)^n = 1. \quad (51)$$

This suggests that continuous observation ensures the initial state $|M\rangle$ remains undecayed, given the survival probability nearing one.

B Contour deformation

This section shows how two contours in Fig.1 are equivalent. We begin by adding a large contour shown as a dotted line in Fig.9(a). This large contour does not contribute to the overall integral (28) because of the exponential in the integrand $e^{zt/\hbar}$, which exponentially suppresses the additional contour.

Next, we add extra contour around the branch cut, shown as solid lines in Fig.9(b). Because of the extra contour, the overall integral (28) now has an extra contribution:

$$\int_{-iR+\sigma}^{iR+\sigma} \dots + \int_{\text{BC}} \dots \quad (52)$$

Since the contour shown in Fig.9(b) is closed, we can use the Cauchy theorem to deform the contour to a closed contour around the pole shown in Fig.9(d).

Finally, we must subtract the extra contribution from the branch cut by adding another contour around the branch cut shown in Fig.9(c), but in the opposite direction to the one added in Fig.9(b). The resulting contour shown in Fig.9(b) is our final result.

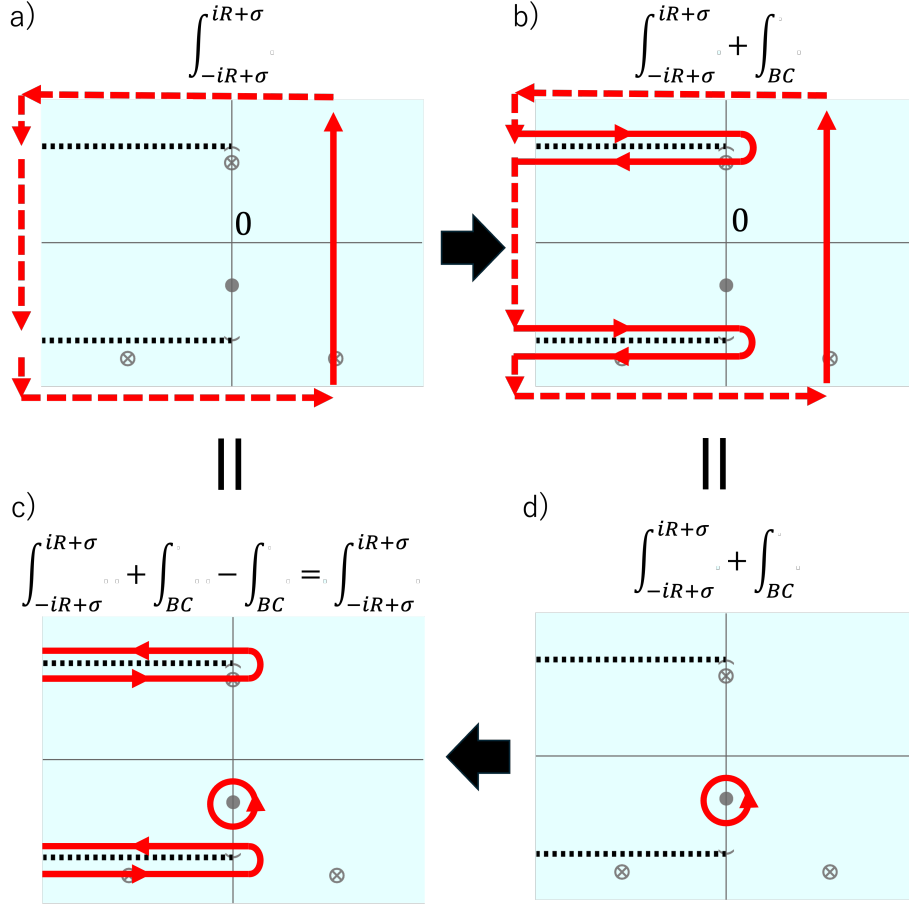


Figure 9: Showing the process of contour deformation to show the equivalence of two contours in Fig.1. For detail explanation of the process, see appendix B.

C Laplace transform

We begin with the master equation (26). Instead of trying to find the memory kernel directly, we perform the Laplace transform $\text{Lap}[\cdot]$, obtaining

$$z\bar{\Phi}(z) - \Phi(0) = -\frac{g^2}{\hbar^2}\bar{\Phi}(z)\text{Lap}[\mathcal{K}(t)](z), \quad (53)$$

where $\bar{\Phi}(z) := \text{Lap}[\Phi(t)](z)$.

Let us look at the Laplace transform of the memory kernel in detail:

$$\begin{aligned} \text{Lap}[\mathcal{K}(t)](z) &= \text{Lap}\left[e^{\frac{i}{\hbar}\omega_0 t} \int_{-L}^L dp \cos\left(\omega_p \frac{t}{\hbar}\right)\right](z) \\ &= \text{Lap}\left[\int_{-L}^L dp \cos\left(\omega_p \frac{t}{\hbar}\right)\right]\left(z - \frac{i}{\hbar}\omega_0\right) \\ &= \int_{-L}^L dp \text{Lap}\left[\cos\left(\omega_p \frac{t}{\hbar}\right)\right]\left(z - \frac{i}{\hbar}\omega_0\right). \end{aligned}$$

In the second equality, we have used one of the properties of the Laplace transform, while in the last equality, we have used the definition of the Laplace transform. The Laplace transform of the cosine function is known to be

$$\text{Lap}\left[\cos\left(\omega_p \frac{t}{\hbar}\right)\right](\tilde{z}) = \frac{\tilde{z}\hbar^2}{\tilde{z}^2\hbar^2 + \omega_p^2} = \frac{\tilde{z}\hbar^2}{\tilde{z}^2\hbar^2 + m^2 + p^2}, \quad (54)$$

where $\tilde{z} \equiv z - (i/\hbar)\omega_0$. Integrating this quantity is much easier than the memory kernel (26), and we thus find

$$\int_{-L}^L dp \frac{\tilde{z}\hbar^2}{\tilde{z}^2\hbar^2 + m^2 + p^2} = \frac{2\hbar^2\tilde{z}\text{Arctan}\left(\frac{L}{\sqrt{m^2 + \tilde{z}^2\hbar^2}}\right)}{\sqrt{m^2 + \tilde{z}^2\hbar^2}}. \quad (55)$$

Then the Laplace transformed master equation (53) becomes

$$z\bar{\Phi}(z) - \Phi(0) = -\frac{g^2}{\hbar^2} \frac{2\hbar^2\tilde{z}\text{Arctan}\left(\frac{L}{\sqrt{m^2 + \tilde{z}^2\hbar^2}}\right)}{\sqrt{m^2 + \tilde{z}^2\hbar^2}} \bar{\Phi}(z). \quad (56)$$

Rearranging the above equation, we find

$$\bar{\Phi}(z) = \left(z + 2g^2 \frac{\tilde{z}\text{Arctan}\left(\frac{L}{\sqrt{m^2 + \tilde{z}^2\hbar^2}}\right)}{\sqrt{m^2 + \tilde{z}^2\hbar^2}} \right)^{-1} \Phi(0). \quad (57)$$

The final solution is found by the inverse Laplace transform

$$\Phi(t) = \text{Lap}^{-1} [\bar{\Phi}(z)] (t). \quad (58)$$

Once again, utilizing the shifting relation of the Laplace transform $\text{Lap}^{-1} [f(z - a)] (t) = e^{at}\text{Lap}^{-1} [f(z)] (t)$, we have

$$\Phi(t) = e^{\frac{i}{\hbar}\omega_0 t} \text{Lap}^{-1} \left[\bar{\Phi} \left(z + \frac{i}{\hbar}\omega_0 \right) \right] (t), \quad (59)$$

where the function inside the inverse Laplace transform is

$$\bar{\Phi} \left(z + \frac{i}{\hbar}\omega_0 \right) = \left(z + i\frac{\omega_0}{\hbar} + 2g^2 \frac{z\text{Arctan}\left(\frac{L}{\sqrt{m^2 + z^2\hbar^2}}\right)}{\sqrt{m^2 + z^2\hbar^2}} \right)^{-1} \Phi(0). \quad (60)$$

The inverse Laplace transform can be evaluated by the Bromwich integral, and we thereby find the formal solution to the master equation (21):

$$\begin{aligned} \Phi(t) &= e^{\frac{i}{\hbar}\omega_0 t} \lim_{R \rightarrow \infty} \int_{-iR+\sigma}^{iR+\sigma} \frac{dz}{2\pi i} e^{zt} \left(z + i\frac{\omega_0}{\hbar} + 2g^2 \frac{z\text{Arctan}\left(\frac{L}{\sqrt{m^2 + z^2\hbar^2}}\right)}{\sqrt{m^2 + z^2\hbar^2}} \right)^{-1} \Phi(0) \\ &= e^{\frac{i}{\hbar}\omega_0 t} \lim_{R \rightarrow \infty} \int_{-iR+\sigma}^{iR+\sigma} \frac{dz}{2\pi i} e^{z\frac{t}{\hbar}} \left(z + i\omega_0 + 2g^2 \frac{z\text{Arctan}\left(\frac{L}{\sqrt{m^2 + z^2}}\right)}{\sqrt{m^2 + z^2}} \right)^{-1} \Phi(0) \end{aligned} \quad (61)$$

where in the last equality, we have rescaled the integration variable by \hbar .

References

- [1] H.-P. Breuer, F. Petruccione, et al. *The theory of open quantum systems*. Oxford University Press on Demand, 2002.
- [2] C. Chiu, E. Sudarshan, and B. Misra. Time evolution of unstable quantum states and a resolution of zeno's paradox. *Physical Review D*, 16(2):520, 1977.

- [3] S. Garmon, T. Petrosky, L. Simine, and D. Segal. Amplification of non-markovian decay due to bound state absorption into continuum. *Fortschritte der Physik*, 61(2-3):261–275, 2013.
- [4] B. Garraway. Nonperturbative decay of an atomic system in a cavity. *Physical Review A*, 55(3):2290, 1997.
- [5] A. González-Tudela and J. I. Cirac. Exotic quantum dynamics and purely long-range coherent interactions in dirac conelike baths. *Physical Review A*, 97, 4 2018.
- [6] V. Gorini, A. Kossakowski, and E. C. G. Sudarshan. Completely positive dynamical semigroups of n -level systems. *Journal of Mathematical Physics*, 17:821–825, 5 1976.
- [7] S. Gurvitz. Single-electron approach for time-dependent electron transport. *Physica Scripta*, 2015, 10 2015.
- [8] W. M. Itano, D. J. Heinzen, J. J. Bollinger, and D. J. Wineland. Quantum zeno effect. *Physical Review A*, 41:2295–2300, 3 1990.
- [9] L. A. Khalfin. Contribution to the decay theory of a quasi-stationary state, 1958.
- [10] A. G. Kofman, G. Kurizki, and B. Sherman. Spontaneous and induced atomic decay in photonic band structures. *Journal of Modern Optics*, 41:353–384, 2 1994.
- [11] G. Lindblad. Mathematical physics on the generators of quantum dynamical semigroups, 1976.
- [12] I. Mezö. On the structure of the solution set of a generalized euler–lambert equation. *Journal of Mathematical Analysis and Applications*, 455(1):538–553, 2017.
- [13] F. Minganti, A. Miranowicz, R. W. Chhajlany, and F. Nori. Quantum exceptional points of non-hermitian hamiltonians and liouvillians: The effects of quantum jumps. *Physical Review A*, 100(6):062131, 2019.
- [14] B. Misra and E. G. Sudarshan. The zeno’s paradox in quantum theory. *Journal of Mathematical Physics*, 18(4):756–763, 1977.
- [15] S. Nakajima. On quantum theory of transport phenomena-steady diffusion, 1958.
- [16] A. Nishino and N. Hatano. Exact time-evolving scattering states in open quantum-dot systems with an interaction: Discovery of time-evolving resonant states. *Journal of Physics A: Mathematical and Theoretical*, 57(24):245302, 2024.
- [17] R. E. A. C. Paley and N. Wiener. Fourier transforms in the complex domain. *Monatshefte für Mathematik und Physik*, 44:A8–A9, 12 1936.
- [18] J. Redondo-Yuste, M. B. D. Paz, P. A. Huidobro, and A. González-Tudela. Quantum electrodynamics in anisotropic and tilted dirac photonic lattices. *New Journal of Physics*, 23, 10 2021.
- [19] A. Rivas and S. F. Huelga. *Open quantum systems*, volume 10. Springer, 2012.

- [20] C. Rothe, S. I. Hintschich, and A. P. Monkman. Violation of the exponential-decay law at long times. *Physical Review Letters*, 96:163601, 4 2006.
- [21] E. Rutherford and F. Soddy. Xxxiii.—the radioactivity of thorium compounds. i. an investigation of the radioactive emanation. *Journal of the Chemical Society, Transactions*, 81:321–350, 1902.
- [22] R. Zwanzig. Ensemble method in the theory of irreversibility. *The Journal of Chemical Physics*, 33:1338–1341, 1960.